Wave Motion 51 (2014) 389–404

Contents lists available at ScienceDirect

Wave Motion

journal homepage: www.elsevier.com/locate/wavemoti

Inverse problems of 3D ultrasonic tomography with complete and incomplete range data

A.V. Goncharsky, S.Y. Romanov *, S.Y. Seryozhnikov

Lomonosov Moscow State University, Moscow, Leninskiye Gory, 1, build.4, 119991, Russia

HIGHLIGHTS

- Efficient methods are proposed for solving inverse problems of 3D ultrasonic tomography.
- The inverse problem is viewed as a coefficient inverse problem for the wave equation.
- Algorithms are based on the direct computation of the gradient of the residual functional.
- Algorithms are implemented on supercomputers.

ARTICLE INFO

Article history:
Received 12 May 2013
Received in revised form 9 October 2013
Accepted 14 October 2013
Available online 25 October 2013

Keywords:
Ultrasonic tomography
3D coefficient inverse problems
Supercomputer

ABSTRACT

The paper focuses on the development of efficient methods for solving inverse problems of 3D ultrasound tomography as coefficient inverse problems for the wave equation. The idea of standard tomographic approaches to solving tomography problems is to analyze the 3D objects by their two-dimensional cross sections. This scheme is perfectly implemented in the case of X-ray tomography. Unlike X-ray tomography, ultrasonic tomography has to deal with diffraction and refraction effects, which limit the possibility of solving 3D problems by analyzing 2D cross sections. We propose efficient methods for solving inverse problems of ultrasound tomography directly in the 3D formulation. The proposed algorithms are based on the direct computation of the gradient of the residual functional. The algorithms are primarily oriented toward the development of ultrasound tomographs for differential diagnosis of breast cancer. Computer simulations demonstrated the high efficiency of the developed algorithms. The algorithms are implemented on GPU-based supercomputers. We analyze various schemes of 3D ultrasonic tomographs including those without rotating elements and with fixed positions of the sources and receivers. The algorithms developed can be used for solving inverse problems of seismology, acoustics, and electromagnetic sounding.

1. Introduction

This study focuses on the problems of the development of high-resolution ultrasound tomographs. Currently, research in this field is conducted in Germany, the USA, Japan, and Russia. Prototype ultrasound tomographic facilities have been developed for medical diagnostics [1–8]. However, despite the evident progress demonstrated at the prototyping stage, no mass production of dedicated ultrasound tomographs has yet started. We believe that several problems have to be addressed to approach mass production and the use of ultrasound tomographs. Below we list some of them.

As is well known, X-rays, which were discovered in late XIX century, almost immediately came to be used as a diagnostic tool in medicine. However, it took 70 years for the first X-ray tomographs to be produced, which have become indispensable

* Corresponding author. Tel.: +7 4959392759.
E-mail addresses: gonchar@srcc.msu.ru (A.V. Goncharsky), romanov60@gmail.com (S.Y. Romanov), s2110sj@gmail.com (S.Y. Seryozhnikov).

0165-2125/$ – see front matter © 2013 Elsevier B.V. All rights reserved.
http://dx.doi.org/10.1016/j.wavemoti.2013.10.001

in medical diagnostics. The main result of X-ray tomography is that it allows the resolution to be increased by a factor of several tens. Dedicated sources, receivers, and experimental designs have been developed to this end, as well as algorithms for solving inverse problems of X-ray tomography, which reduced the study of 3D objects to solving two-dimensional problems of reconstructing the 2D cross sections of the object. This approach is based on the physical principle of the propagation of X-rays. X-rays can be absorbed, but they are very difficult to deflect. The refraction index for soft X-ray radiation is equal to $\sim (1 - 1 \cdot 10^{-5})$, and this means that when a 3D object is scanned by an X-ray beam propagating in a plane, the beam remains in the same plane. The latter property of X-ray radiation allows three-dimensional objects to be diagnosed layer by layer via X-ray tomography.

The situation is totally different in wave tomography using, e.g., ultrasound radiation. Diffraction, refraction, and reflection are significant effects in this case, because the wavelength of, e.g. ultrasound radiation exceeds that of soft X-ray radiation by more than a factor of 10^5. However, most of the studies aimed at the development of algorithms for solving inverse problems of ultrasound tomography are based on the layer-by-layer paradigm [9–15]. Glide, Duric, and Littrup [9,10] consider the inverse problem in 2D version with the ring geometry of the registration system. Huang and Quan [11] use the layer-by-layer approach to address the inverse problem of transmission tomography reconstruction. Backushinsky, Goncharskii, and Romanov [16,17] show how the technique of Green's functions can be used to reduce the wave tomography problems to a nonlinear set of integral equations. Schmidt et al. [12] use a linearized representation of these integral equations to address two-dimensional problems of the reconstruction of a speed cross section in ultrasound tomography. Similar linearized procedures are used in inverse problems of geophysics, where they are known as the Kirchhoff migration method [13].

On our earlier paper [18] we developed efficient methods for solving inverse problems of ultrasound tomography as coefficient inverse problems for the wave equation in the layer-by-layer version. We also developed efficient numerical algorithms for reconstructing two-dimensional cross sections of objects studied. Algorithms for solving inverse problems as coefficient problems for the wave equation are rather computationally intensive even in the two-dimensional case, and supercomputers are needed to implement them.

Unfortunately, in the case of a layer-by-layer model such wave effects as refraction, diffraction, and rereflection between inhomogeneities may distort the shape of the reconstructed inhomogeneity and produce artifacts. In this paper, we illustrate these effects by computing a test model problem with the 3D direct problem of wave propagation in inhomogeneous medium solved using an independent method. We use a homogeneous sphere as a test object. Such an inhomogeneity allows an analytical solution to be derived in the form of a series of special functions. To assess the quality of layer-by-layer models, we solved the 2D version of the inverse problem in several layers. The results obtained show that layer-by-layer schemes can, in principle, be used in ultrasound tomography. However, interpretation of the data obtained in terms of such models should take into account both geometric distortions and the artifacts due to the layer-by-layer nature of the model. The above complications disappear if the inverse problem is solved explicitly in the 3D version.

Note also that the layer-by-layer model is in principle incapable of accounting for rereflection between inhomogeneities located in different layers. The 3D model allows for these effects automatically. Hence from the physical viewpoint explicit 3D algorithms should in every respect be preferred to layer-by-layer models when it comes to solving inverse problems of wave tomography [15].

The question arises: why is the layer-by-layer approach so popular among the authors of published studies? The point is that solving 3D problems as coefficient inverse problems is a much more computationally intensive task than applying an algorithm based on the layer-by-layer model. To ensure high resolution, the inverse problem should be solved on a sufficiently fine mesh (with at least 400 points along each of the coordinates) both in the 2D and 3D approach. It suffices to remark that the number of unknowns in the explicit 3D model exceeds 10^{11} in the case considered. It is with so many unknowns that one has to solve a complex nonlinear inverse problem.

Only a few studies attempt to solve coefficient inverse problems in the explicit 3D formulation [19–23]. Beilina and Klibanov [19] analyze the three-dimensional coefficient problem where a 3D object is illuminated by electromagnetic radiation. The reflected electromagnetic wave is registered on the source side. The reconstruction capabilities in this case are limited because of the limited range of angles. In this respect the situation is much better in problems of ultrasound tomography when applied to breast cancer diagnosis, because the diagnosed object can be studied from different sides. It cannot be sounded only from one side (that of breast).

Wiskin et al. [20] and André et al. [21] solve the 3D problem of ultrasound tomography stage by stage. At the first stage the transmission part of the inverse problem is solved in the parabolic equation approximation. Parabolic approximation allows diffraction and refraction to be taken into account only for small deflection angles, and therefore at the first stage the inverse problem is solved using the data recorded on the side of the object opposite to the source. Reflection data are used at the second stage of the algorithm. Sounding is performed for several frequencies.

Natterer [22] solves the inverse problem of 3D ultrasound tomography in the Helmholtz equation approximation. The object is irradiated from different sides by planar ultrasound waves of a certain frequency. Numerical computations performed on a $65 \times 65 \times 65$ grid cannot produce high-resolution images.

The truly breakthrough results could be obtained in the solution of coefficient inverse problems of ultrasound tomography when it was possible to write the exact formula for the gradient of the residual functional by solving the conjugate problem. Various flavors of this approach are represented in studies [24,25,19,18,26]. Efficient algorithms for the approximate solution can be developed if we know how to compute the gradient of the residual functional. This study is concerned with the development of efficient methods for solving inverse problems directly in the 3D formulation using the

exact formula for the gradient. This study investigates ultrasonic tomographs for differential diagnosis of soft tissue cancer, primarily, the breast cancer. The inverse problem is formulated as the coefficient problem of reconstructing the sound speed function $v(x, y, z)$ in soft tissue.

Another important result of this study is associated with the development of efficient algorithms for solving coefficient inverse problems with incomplete range data, where the object studied cannot be sounded from all directions [27]. It is evident that narrowing the range of sounding angles results in a worse reconstruction. In this respect the situation is most challenging in seismology and in problems of electromagnetic sounding of subsurface Earth layers, where both the sources and detectors are located in the same plane. The situation is much better in ultrasound tomography when applied to diagnosing breast cancer, although in this case we also have to deal with the incomplete data [28].

Ultrasound tomography is the ideal test ground for tomographic algorithms in wave models. In medicine there are standard devices for ultrasound diagnosis, where the object is sounded from one side only. The aim of the ultrasound tomography is to increase the resolution of ultrasound technologies both in terms of space coordinates and the sound speed in the inhomogeneity. This paper focuses on determining the capability limits of the currently designed ultrasound tomographs. An important result of our work is the demonstration of the capabilities of numerical algorithms for solving coefficient inverse problems explicitly in the 3D case. One of the main tasks of our study is to analyze the optimum location of sources for 3D ultrasound tomography schemes with incomplete range data.

A typical task one has to face when developing iterative algorithms for the approximate solution of ultrasound tomography problems is the proper choice of the initial approximation. One of the options is to choose solutions of the linearized approximations of Born and Rytov [29]. However, we believe the most natural initial approximation in iterative processes in ultrasound tomography problems to be a constant function, because it requires no additional computations. It is this initial approximation that we use in all model computations performed in this study.

2. Formulation and methods of solution for the inverse problem

There are different formulations of coefficient inverse problems for hyperbolic equations [25,19,30,18]. In this paper, we examine the inverse problem in the scalar wave approximation. Consider the wave equation that describes some acoustic field $u(r, t)$ during time $(0, T)$ in the domain $\Omega \subset R^N$ $(N = 3)$ bounded by the surface S with a point source located at point r_0

$$c(r)u_{tt}(r, t) - \Delta u(r, t) = \delta(r - r_0) \cdot f(t) \tag{1}$$

$$u(r, t = 0) = u_t(r, t = 0) = 0 \tag{2}$$

$$\partial_n u|_{ST} = p(r, t). \tag{3}$$

Here $c^{-0.5}(r)$ is the wave velocity in the medium; $r \in R^3$, the position of the point in space, and Δ, the Laplacian operator with respect to r. The pulse generated by the source is described by function $f(t)$; $\partial_n u|_{ST}$ is the derivative along the normal to the surface S in the domain $S \times (0, T)$, and $p(r, t)$, a known function. We assume that inhomogeneities of the medium are due to velocity variations exclusively, whereas the velocity outside the inhomogeneity domain is equal to $c(r) \equiv$ const, where *const* is known.

Wave equation (1) effectively describes such wave effects as diffraction, refraction, and rereflection in non-attenuating media. However, even in the framework of this very simple model the solution of inverse problems of ultrasound tomography involves solving ill-posed problems. Problem (1)–(3) is known to define $u(c)$ as an implicit function of $c(r)$. The inverse problem consists in reconstructing function $c(r)$ that describes the inhomogeneity from experimental measurements of wave $U(s, t)$ at the domain boundary S during time $(0, T)$ for different positions r_0 of the source.

Let us now introduce the following functional of residual

$$\Phi(u(c)) = \frac{1}{2}\,\|u|_{ST} - U\|^2 = \frac{1}{2}\int_0^T \int_S (u(s, t) - U(s, t))^2 \; dsdt, \tag{4}$$

where $\|\cdot\|^2$ is the squared norm in the $L_2(S \times (0, T))$ space, and $U(s, t)$ are the experimental data at the domain boundary S during time $(0, T)$.

The breakthrough results in solving the problems of ultrasound tomography are associated with the computation of the gradient of functional $\Phi(u(c))$. Formulas for the gradient of functional $\Phi(u(c))$ in similar formulations were derived by Natterer and Wubbeling [25] and Beilina and Klibanov [19]. We derived the formulas for the gradient of functional $\Phi(u(c))$ in the current formulation in our earlier papers [26,18]. The gradient $\Phi'(u(c))$ is the part of the increment of functional $\Phi(u(c))$ (4) that is linear with respect to arbitrary variation dc. In this case

$$\Phi'_C(u(c)) = \int_0^T w_t(r, t)u_t(r, t)dt. \tag{5}$$

Here $u(r, t)$ is the solution of problem (1)–(3), and $w(r, t)$, that of the following, "conjugate" problem (6)–(8) for given $c(r)$

$$c(r)w_{tt}(r, t) - \Delta w(r, t) = 0, \tag{6}$$

$$w(r, t = T) = w_t(r, t = T) = 0, \tag{7}$$

$$\partial_n w|_{ST} = u|_{ST} - U. \tag{8}$$

We further impose the boundary condition $\partial_n w|_{ST} = 0$ at the points of boundary S, where no experimental data are available. Thus, both the main and the "conjugate" problems have to be solved to compute the gradient of the functional.

Given Φ'_C from (5), various iterative schemes can be developed for minimizing the residual functional (4). Numerical methods employed in this paper use the steepest descent technique to numerically solve at each iteration the problem of one-dimensional minimum search in the gradient direction. Other gradient methods including regularized iterative procedures [31] can also be used to this end.

3. Numerical algorithms for solving the inverse problem

We use the finite difference method on uniform meshes to solve the three-dimensional inverse problem. In this formulation solving differential wave equations reduces to solving difference equations. We introduce the following uniform mesh in the domain of function arguments

$$v_{ijlk} = \left\{(x_i, y_j, z_l, t_k) : x_i = ih, 0 \le i < n; y_j = jh, 0 \le j < n; z_l = lh, 0 \le l < n; t_k = k\tau, 0 \le k < m\right\},$$

where h and τ are the mesh steps in the spatial and time directions, respectively. Parameters h and τ are related by the Courant stability condition $c^{-0.5}\tau < h/\sqrt{3}$, where $c^{-0.5}(r)$ is the wave velocity.

We use the following approximations to the second-order derivatives in Eq. (1)

$$u_{tt}(x_i, y_j, z_l, t_k) = \frac{u_{ijlk+1} - 2u_{ijlk} + u_{ijlk-1}}{\tau^2},$$
$$\Delta u(x_i, y_j, z_l, t_k) = \frac{u_{i+1jlk} - 2u_{ijlk} + u_{i-1jlk}}{h^2} + \frac{u_{ij+1lk} - 2u_{ijlk} + u_{ij-1lk}}{h^2} + \frac{u_{ijl+1k} - 2u_{ijlk} + u_{ijl-1k}}{h^2},$$

where $u_{ijlk} = u(x_i, y_j, z_l, t_k)$. In the source-free domain we obtain the following explicit difference scheme for differential equation (1)

$$c_{ijl}\frac{u_{ijlk+1} - 2u_{ijlk} + u_{ijlk-1}}{\tau^2} - \frac{u_{i+1jlk} - 2u_{ijlk} + u_{i-1jlk}}{h^2} - \frac{u_{ij+1lk} - 2u_{ijlk} + u_{ij-1lk}}{h^2} - \frac{u_{ijl+1k} - 2u_{ijlk} + u_{ijl-1k}}{h^2} = 0. \tag{9}$$

Or we extract the term u_{ijlk+1} corresponding to the $(k+1)$th time layer to derive the following formula for computing the propagation of the sound wave by time layers ("direct propagation")

$$u_{ijlk+1} = u_{ijlk}\left(2 - \frac{8\tau^2}{c_{ijl}h^2}\right) + \frac{(u_{i+1jlk} + u_{i-1jlk})\tau^2}{c_{ijl}h^2} + \frac{(u_{ij+1lk} + u_{ij-1lk})\tau^2}{c_{ijl}h^2} + \frac{(u_{ijl+1k} + u_{ijl-1k})\tau^2}{c_{ijl}h^2} - u_{ijlk-1}. \tag{10}$$

Here c_{ijl} is the $c(x_i, y_j, z_l)$ value at point (x_i, y_j, z_l). We adopt perfectly absorbing boundary conditions [32] for our computer simulations

$$\partial_n u|_{ST} = -c^{0.5}\,\partial_t u|_{ST}. \tag{11}$$

The "backpropagation" scheme for w can be written in a similar way. Time T is chosen to be sufficiently large for all the main reflections and rereflections from the object studied to reach the receivers. In difference approximation, e.g., at face $z = z_n$ (for the boundary S having the shape of a cube boundary) condition (8) can be written as follows

$$\frac{w_{ijl+1k} - w_{ijl-1k}}{2h} = u_{ijlk} - U_{ijlk}.$$

In our simulations the domain studied is surrounded by a homogeneous medium inside which a source is located. The propagation of the sounding pulse in a homogeneous medium for wave equation (1) is known to be described by function

$$u(r, r_0, t) - \frac{1}{4\pi\,\|r - r_0\|} f\left(t - \|r - r_0\|\, c_0^{0.5}\right), \tag{12}$$

where $\|\cdot\|$ is the distance of point r from the location of the source, r_0. This formula can be used to compute $u(r, t)$ and $u_t(r, t)$ at some small t. We report the form of the sounding pulse in Section 5.

We compute the gradient (5) of functional (4) by the following difference formula

$$grad_{ijl} = \sum_{k=0}^{m} \frac{u_{ijlk+1} - u_{ijlk}}{\tau}\frac{w_{ijlk+1} - w_{ijlk}}{\tau}\tau. \tag{13}$$

Let us now describe the steepest descent algorithm for the numerical solution of the inverse problem. We construct the iterative sequence $c^{(n)}$ for minimizing the functional of residual (4) as follows:

(1) we adopt $c^{(0)} = c_0 = const$ as our initial approximation;
(2) we solve direct problem (1)–(3) for $c^{(0)}$ in the difference approximation and use the explicit difference scheme (9) to compute the $u(r, t)$ value for each detector;
(3) we solve the conjugate problem (6)–(8) for function $u(r, t)$ for each detector in the difference approximation. As a result, we obtain $w(r, t)$ at each mesh point;
(4) we use the resulting $u(r, t)$ and $w(r, t)$ values to compute the gradient $\Phi'_C(u(c^{(0)}))$ (5) of the functional by formula (13);
(5) given the gradient at point $c^{(0)}$, we minimize $\Phi(c^{(0)} - \gamma\Phi'_C(c^{(0)}))$ as a function of parameter γ in the domain $\gamma > 0$;
(6) we adopt the point of minimum of the functional as our new iteration $c^{(1)}$. The process returns to stage (1);

Similar algorithms are used for the iteration process both in the 2D and 3D cases [18].

The number of unknowns in the finite-difference approach is $\sim n^{N+1}$, where n is the number of computational mesh points along one direction and $N = 2, 3$, the dimension of the problem ($N = 2$ corresponds to the layer-by-layer scheme). The number of unknowns for the 3D problem increases by a factor of n compared to that of the 2D problem. Thus for $n = 400$ the number of unknowns in the explicit 3D model exceeds 10^{11} in this case. Supercomputers allow computations to be efficiently parallelized thereby reducing the computing time by a factor of several hundred.

However, although solving 3D problems is a very difficult task, we believe this approach to be most promising, because it allows the problem to be solved with the allowance for refraction and diffraction effects, and rereflection in three-dimensional space. It goes without saying that two-dimensional problems are easier to solve from the computational viewpoint, however, the underlying physical model is less representative of reality. For example, the layer-by-layer model may take into account rereflection within the layer, but fails to allow for rereflections between inhomogeneities located in different layers, etc. The 3D wave model describes these effects automatically.

4. Supercomputer technologies for implementing numerical methods for solving inverse problems of ultrasound tomography

Inverse problems of ultrasound tomography in three-dimensional space are very computer intensive. To achieve sufficiently high resolution, the reconstruction of the three-dimensional function $c(x, y, z)$ has to be performed on a $500 \times 500 \times 500$ mesh. This means solving a nonlinear coefficient inverse problem with more than 100 million unknowns. To save computing resources, we solved our model problems on a $400 \times 400 \times 400$ mesh.

The proposed computing procedure for solving the inverse problem of ultrasound tomography has high degree of data parallelism, because the new function values for the new time layer at all mesh points, except those located at the boundary, are computed in accordance with the same scheme both in the "direct" and "conjugate" problem, and are independent of each other. Such algorithms are referred to as SIMD (Single instruction-multiple data) algorithms, and auxiliary vector processors came to be widely used to implement them in recent years. These devices have progressed most impressively as parts of graphical processing units (GPU) due to their wide use and hence low cost.

Modern GPUs combine several processing cores (or multiprocessors, MP) with an array of high-speed graphical memory (GDDR) on a single chip. A video card typically contains 10–20 cores, each capable of processing several hundred (typically 512) parallel threads, making it possible to achieve enormous peak performance of several TFlops (without memory access).

A GPU has typically 1–2 Gb memory and throughput of several hundred (typically 160–250) Gb/s, whereas the system memory (RAM) commonly used in computers has a throughput of 8–15 Gb/s. This circumstance is of great importance for our task with an explicit difference scheme, because it is not very arithmetically intensive, i.e., it involves a rather small number of arithmetic operations and many memory access operations. Thus the mere use of faster GPU memory allows the computations to be sped up by a factor of 20–30 compared to a PC. Real acceleration can amount to a factor of 50–100 because of more efficient compilation of GPU code.

The weakest point of the GPU is its communication with the host system, which is usually implemented via the PCI Express interface. This interface has a relatively low throughput (several Gb/s), which makes it unreasonable to run with GPU tasks requiring permanent access to more memory than installed on the GPU. We took this constraint into account when running our computations.

We used the OpenCL interface for GPU programming, because it is more universal than NVidia CUDA interface and can be applied to a wider class of parallel computing devices. In addition, OpenCL also allows easy synchronization of the CPU and GPU operation.

To solve the task, we used the supercomputer of the Supercomputing Center of Lomonosov Moscow State University [33]. We performed our computations on 13 GPUs on NVIDIA Tesla X2070 graphics card with 14 multiprocessors, about 6.0 GB of global memory, 48 kB of shared memory per thread block, and with each thread block having a size of 32×16. The use of supercomputer allowed us to solve the inverse problem of ultrasonic tomography by reconstructing the three-dimensional function of velocity $v(x, y, z)$ in about 1 h for the adopted parameter values.

GPU-based supercomputers were already used before to solve ultrasonic tomography tasks involving the reconstruction of three-dimensional objects by their two-dimensional cross sections [14].

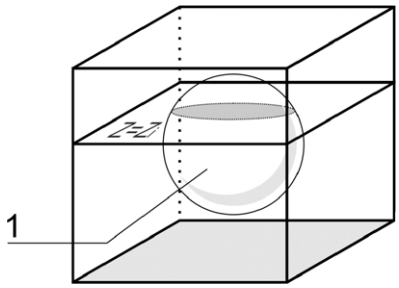

Fig. 1. Scheme of the computational experiment.

5. Model computations

5.1. Model problem 1. Layer-by-layer reconstruction of a 3D object

The aim of the computations made within the framework of model problem 1 is to study the feasibility of using layer-by-layer schemes for tomographic reconstruction of 3D objects in wave tomography. We adopt three-dimensional sphere (Fig. 1) as our test object, because the solution of the direct problem for a spherically symmetric object can be written explicitly in the form of an expansion in special functions [34]. The fact that the direct problem can be solved analytically makes the simulation "cleaner" and, in addition, allows us to control the numerical methods used for solving the direct problem.

The computer simulation consisted in the following. The sphere denoted by numeral 1 in Fig. 1 is irradiated from four lateral sides by plane waves. We then choose a set of horizontal cross-sections $z = z_i$ $(i = 1, \ldots, 5)$ of the sphere and solve analytically the 3D problem of determining the scattered field at the boundary of the computational cube for each plane $z = z_i$. We then use the data obtained as the input to solve the inverse 2D problem in the cross section using methods described by Goncharsky and Romanov [18], and compare the resulting solution with the known cross section of the sphere by the corresponding plane.

Analytical methods for solving the problem of scattering by sphere $\Omega \subset R^3$ are well known [34].

We assume that the sound speed inside the sphere with boundary S is equal to $c(r) \equiv c_\Omega = const$. The sound speed outside the sphere is equal to $c(r) \equiv c_0 = const$, and mass density inside and outside the sphere are the same and equal to $\rho = const$. We further assume that the incident field $u^i(r)(r \notin \Omega \subset R^3)$ is a plane wave propagating along the OZ axis: $u^i(r) = e^{-ikz}$. We denote the total field outside $\Omega(r \notin \Omega \subset R^3)$ as $u(r)$. It is equal to the sum of the incident wave and the unknown scattered field $u^s(r)$, i.e., $u(r) = u^i(r) + u^s(r)$. These functions obey the Helmholtz equation outside the sphere with wavenumber $k = \omega/c_0$. We denote the total field inside the sphere as $u^\Omega(r)$. It satisfies the Helmholtz equation inside the sphere with wavenumber $k_\Omega = \omega/c_\Omega$. At the boundary S of the sphere both the field $u(r)$ and field $u^\Omega(r)$ satisfy the following conditions [35]:

$$u = u^\Omega \quad \text{and} \quad \frac{1}{\rho} \cdot \frac{\partial u}{\partial \nu} = \frac{1}{\rho} \cdot \frac{\partial u^\Omega}{\partial \nu},$$

where $\frac{\partial}{\partial \nu}$ is the outward-pointing normal derivative at boundary S.

The problem of scattering by a sphere consists in finding the scattered field $u^s(r)$ outside sphere $\Omega \subset R^3$ that satisfies the Sommerfeld radiation conditions at infinity. The solution of this problem can be written in analytical form.

Let us introduce spherical coordinates such that the point with Cartesian coordinates (x, y, z) has coordinates $(|r|, \theta, \varphi)$. The incident field can be written in the form of the following series

$$u^i(|r|, \theta) = e^{-ik|r|\cos\theta} = \sum_{m \geq 0} \delta_m \cdot (-i)^m \cdot T_m \cdot j_m(k_0 |r|),$$

where $T_m = P_m(\cos\theta)$, $P_m(x)$ are the Legendre polynomials, $\delta_m = 2m + 1$, $j_m(x) = \sqrt{\frac{\pi}{2x}} \cdot J_{m+\frac{1}{2}}(x)$ is the Bessel function of the first kind. The solution of the Helmholtz equation satisfying the radiation condition outside domain Ω then has the following form:

$$u^s(|r|, \theta) = \sum_{m \geq 0} D_m \cdot \delta_m \cdot (-i)^m \cdot T_m \cdot h_m(k|r|), \tag{14}$$

where

$$D_m = \frac{C \cdot j_m(kR) \cdot j'_m(k_\Omega R) - j'_m(kR) \cdot j_m(k_\Omega R)}{j_m(k_\Omega R) \cdot h'_m(kR) - C \cdot j'_m(k_\Omega R) \cdot h_m(kR)};$$

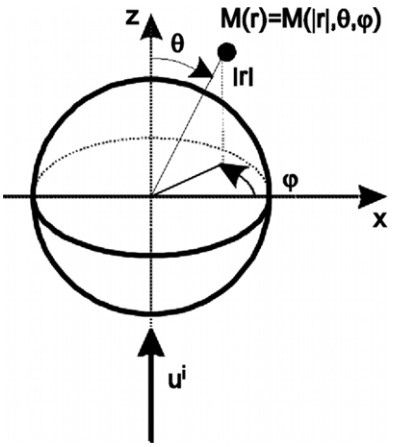

Fig. 2. Derivation of the analytical solution for the scattering problem.

$h_m(x) = \sqrt{\frac{\pi}{2x}} \cdot H_{m+\frac{1}{2}}(x)$ is the spherical Hankel function of the second kind. Inside domain Ω the solution of the Helmholtz equation has the following form:

$$u^{\Omega}(|r|, \theta) = \sum_{m \geq 0} F_m \cdot \delta_m \cdot (-i)^m \cdot T_m \cdot j_m(k|r|),$$

where

$$F_m = \frac{j_m(kR) \cdot h'_m(kR) - j'_m(kR) \cdot h_m(kR)}{j_m(k_{\Omega}R) \cdot h'_m(kR) - C \cdot j'_m(k_{\Omega}R) \cdot h_m(kR)}.$$

We now assume that the incident field is a plane wave having the form of a short pulse propagating along the OZ axis:

$$p^i(r, t) = f\left(t - \frac{z}{c_0}\right).$$

Here function $f(t)$ is nonvanishing in the interval $(t_*, t_* + \tau)$, where τ is the pulse duration. We consider function $f(t)$ as finite Fourier series (15) over the interval $(-T, T)$, where T is chosen based on the condition that the pulse should pass completely across the domain considered. Time $t = 0$ corresponds to the beginning of the passage of the pulse through point $x = y = z = 0$.

$$f(t) = \sum_{n=-N}^{N} f_n \exp(i\omega_n t), \quad \omega_n = \frac{2\pi n}{T}. \tag{15}$$

We can now make use of the fact that both the Helmholtz equation and matching conditions are linear to solve the scattering problem by formulas (14) separately for each harmonic ω_n ($k_n = \omega_n/c_0$) of relation (15) and derive solutions $u^s(r, \omega_n)$. The general solution of the problem on the interval $(-T, T)$ is the sum of the solutions obtained for the harmonics considered.

We performed model computations for the layer-by-layer reconstruction of the 3D object in each of the layers along the z axis for four sources with interreceiver distances no greater than $\lambda/3$, where λ is the pulse length. The sound speed inside and outside the sphere is equal to $c_{\Omega} = 1600$ and $c_0 = 1500$ m/s, respectively; the pulse size is 7 mm, and the radius of the sphere, $R = 6$ cm. Radiation has the form of a plane wave incident onto the inhomogeneity perpendicularly to the Z axis and parallel to the sides of the square (Fig. 2). We performed the computations for the inverse problem in 20×20 cm^2 square cross sections on a 1000×1000 grid in the square considered.

The bottom part of Fig. 3 shows the speed cross sections $c(x, y)$ reconstructed in the selected cross sections $z = 0$ cm, $z = 3$ cm, $z = 4$ cm, $z = 5$ cm, and $z = 6$ cm. Here $z = 0$ passes through the center of the sphere and z increases from left to right. The top part of the figure shows, for comparison, the model cross sections of the sphere for the same z. As is evident from the figure, the reconstructed solution for the $z = 0$ cross section practically coincides with the exact solution. The shape of the cross section practically coincides with that of the inhomogeneity in this cross section. Small artifacts are due both to computational errors in the solutions of both the direct and inverse problems, and to the small number of sources. However, already in the next cross section at $z = 3$ cm the shape of the inhomogeneity is distorted because of refraction, which is even stronger for the $z = 4$ cm and $z = 5$ cm cross sections. Refraction increases with increasing z. Thus at $z = 6$ cm the entire image is nothing but an artifact, given that the exact solution is a mere point.

We therefore conclude that although the layer-by-layer scheme can, in principle, be applied in ultrasound tomography, it distorts the geometric parameters of inhomogeneities, creates artifacts, and produces images that are blurred along

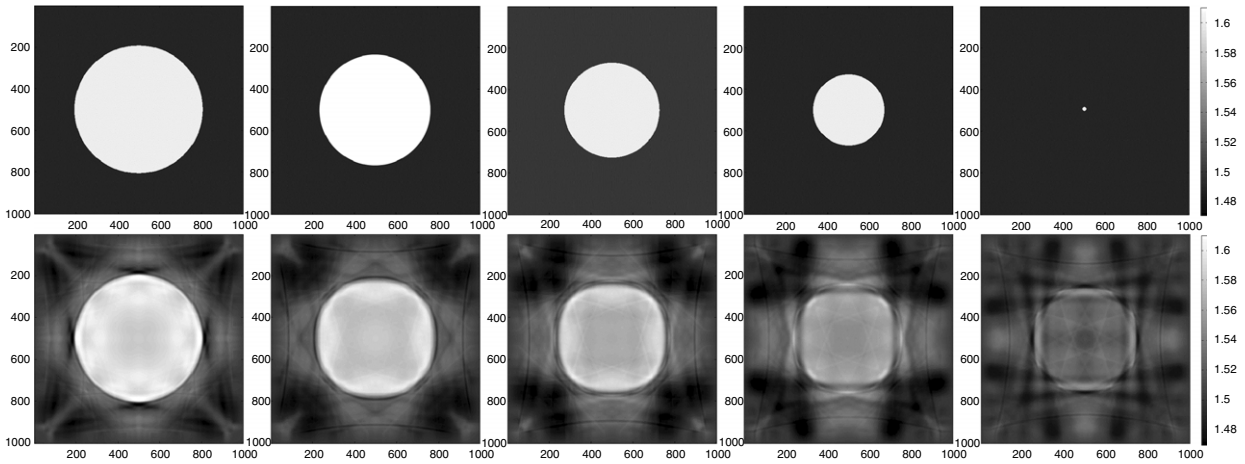

Fig. 3. Model and reconstructed cross sections.

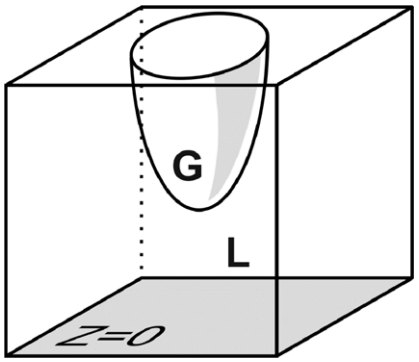

Fig. 4. Experimental design. Here G is the region studied and L, the region with known velocity v_0 of ultrasonic wave propagation.

the z axis—consistent with what was reported in [15]. In a physically rigorous way the problems arising in layer-by-layer tomography are most easily described in terms of ray approximation. Unlike X-ray tomography, rays in wave (e.g., ultrasound) tomography are no more straight lines. Moreover, they are not confined to the plane and this fact restricts the capabilities of layer-by-layer schemes in tomography.

5.2. Model problem 2. Reconstruction of a 3D object in complete and incomplete range of angles

We performed our computations in terms of the mathematical model described by Eq. (1). Fig. 4 shows the scheme of the simulation of ultrasonic tomography diagnostics of region G, which contains irregularities. Region G is located inside a cube and is surrounded by medium L with known velocity $v_0 = const$ of ultrasonic wave propagation. Sources and receivers of ultrasonic pulses are located on the cube faces.

As a phantom for model examinations we used a three-dimensional object of nonuniform structure with a size of up to 100 mm and with variations of ultrasound wave velocity not exceeding 10%. The minimum size of irregularity was 2 mm.

We adopted the following main problem parameters:

(1) wavelength of sounding pulse, $\lambda = 5$ mm;
(2) the horizontal and vertical size of the cube of ultrasound sounding, up to 11 cm;
(3) computations are performed on a uniform mesh inside a cube, the number of mesh points along the horizontal and vertical coordinates is $400 \times 400 \times 400$;
(4) the number of sources varies from 5 to 25;
(5) the interreceiver distance is $\lambda/2$, where λ is the wavelength.

The radiation wavelength is an important parameter in ultrasonic tomography. The wavelength adopted in simulations, 5 mm, exceeds those employed in common ultrasonic examinations. The reason for this choice is that in tomography problems signals on detectors should be highly accurate. Ultrasonic radiation is absorbed in soft tissues, and the absorption depends strongly on frequency, or, which is the same, on wavelength. Simulations show that in the case of small errors

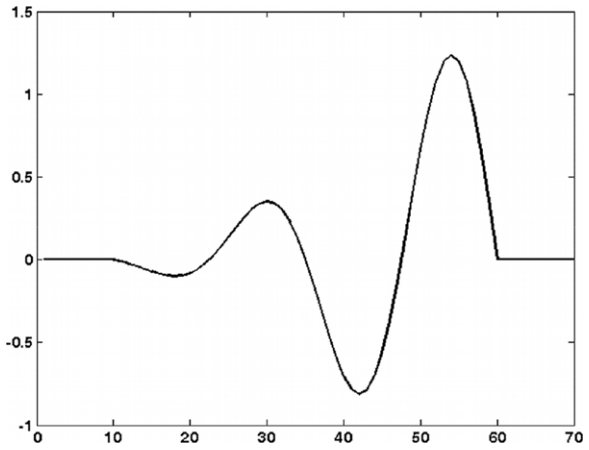

Fig. 5. Plot of a sounding pulse.

in input data the adopted ∼5 mm wavelength range allows cross-section features with sizes smaller than 2 mm to be reconstructed.

The inverse problem considered here is a coefficient inverse problem. The Green function technique can be used to reformulate it into a set of nonlinear Fredholm equations of the second kind [29,16]. The iteration algorithms proposed in this paper are regularizing if the regularization parameter is properly chosen. Our parameter can be the number of iterations set as a function of data errors. The approximate solution derived tends to the exact solution as the error tends to zero. The latter means sufficiently small errors allow arbitrarily high resolution to be achieved. Hence in our case the resolution is determined by the data errors [29]. If the error is fixed the quality of the reconstruction of the sounded object degrades with increasing wavelength.

In the simulations the sounding pulse at some time $t_1 > 0$ is set in the form of a wave spherically propagating in medium L given by the formula

$$\begin{cases} u(r, t_1) = K \exp(-\alpha(r - R_0)^2) \sin\left(\dfrac{4\pi(r - R_0)}{v_0 T}\right), & \text{at } R_0 - v_0 T < r < R_0 \\ u(r) = 0, \quad \text{in all other cases} \end{cases}, \tag{16}$$

where r is the distance from the current point to the pulse source; T, the pulse duration; v_0, the wave propagation velocity in medium L; R_0, the distance from the leading edge of the wave to the pulse source, and $\alpha > 0$ determines the steepness of the pulse envelope, K is the pulse amplitude.

Fig. 5 shows the plot of sounding pulse $u(r, t_1)$ with the following parameters: $K = -1.3$, $\alpha = 0.45$, $R_0 = 10$ mm, $c_0 = 1\,500\,000$ mm/s, and T $= 0.00000666$ s. The sounding pulse at the next time instant $t_1 + \tau$ can be easily found by formula (12). The field strength at time t_1 from formula (16) and at time $t_1 + \tau$ determine the initial conditions of the computations.

Function $u(r, t_1)$ has compact support, whose size is approximately equal to two wavelengths. Real sources are characterized by different shapes of pulses $u(r, t_1)$. The form of the pulse depends on the materials and structure of the sources, and on the electric signal applied to them. In terms of certain models, electric signal can be computed that should be generated and applied to the source in order to obtain the required initial pulse $u(r, t_1)$. A characteristic feature of all pulses $u(r, t_1)$ are certain oscillations (see Fig. 5). The smaller these oscillations, the better. In the ideal case there should be no oscillations.

The relation between the computational mesh interval and the duration of the sounding pulse is such that for every pulse period there are 25 mesh points in spatial coordinates, which ensures good approximation for the numerical computation of Laplacian. The mesh interval in t is determined by the Courant relation $c^{-0.5}\tau < h/\sqrt{3}$, which ensures the convergence of the explicit scheme. We set the Courant parameter equal to 0.25.

Model computations were performed both in the case of full range of angles, where the sources and receivers were located on every side of the object studied, and in the case of incomplete angle range, where neither sources nor receivers can be located at the face $z \geq H$ of the cube. Computations with incomplete angle range are performed to simulate the applied problem of breast cancer diagnosis, because neither the sources, nor the receivers can be arranged on the side of the breast.

Complete angle range.

In model computations with a complete range of angles we used six sources arranged at the centers of each face of the cube, and many receivers covering each face (Fig. 6). The interval between the receivers on cube faces is equal to about $\lambda/2$, where λ is the wavelength.

When simulating the reconstruction of a 3D irregularity we solved the direct problem of the propagation of ultrasonic wave in a three-dimensional region without introducing additional error, by explicit formula (10) with boundary conditions

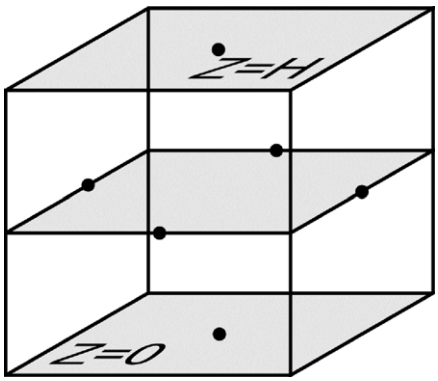

Fig. 6. The layout of sources in the experiment with complete range of angle data.

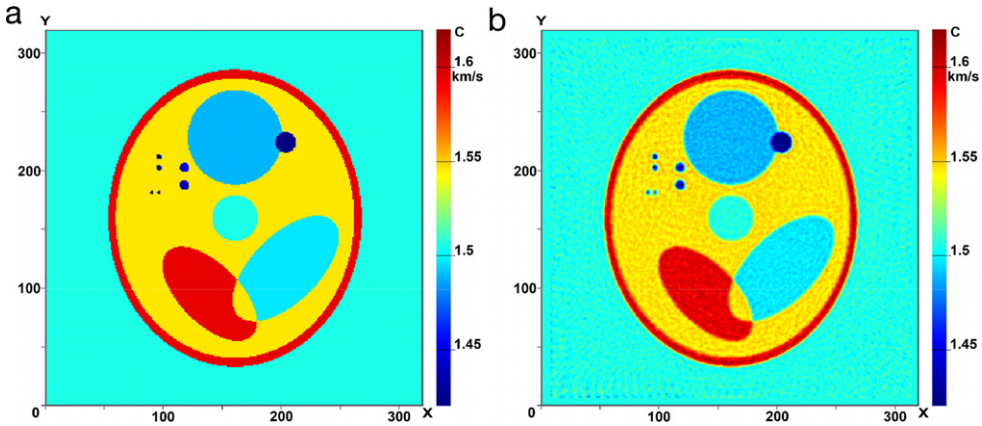

Fig. 7. (a, b). The left- and right-hand panels show the cross sections of the phantom of the 3D object and the reconstructed cross sections of the 3D object, respectively. The cross sections are perpendicular to the Z axis.

Table 1
Values of the residual functional.

Number of iterations	1	5	15	105	230
Residual functional (six sources)	0.011424	0.006348	0.001625	0.000231	0.000147
Computing time, min	1.6	8	24	168	368

(11) and initial conditions specifying the sounding pulse (16). We then used the resulting data to solve the inverse problem of reconstructing the function of wave speed $v\,(x, y, z)$.

Figs. 7–9(a, b) show, for the case of the scalar speed function $v(x, y, z)$ that depends on three space coordinates, the cross sections passing through object G in four different planes perpendicular to the Z axis at different $z = z_i\,(i = 1, \ldots, 3)$. The left-hand panel shows the cross sections of the phantom and the right-hand panel, the resulting reconstructed images. Speed is color coded and the color scale is shown in each image. The reconstructed images are those obtained at the 120th iteration of the iterative process. As is evident from the figures, the quality of reconstruction is very good so that even small irregularities with sizes ∼2 mm are restored fairly well.

Fig. 10 (a, b) shows the cross section passing through the irregularity studied in the plane perpendicular to the X axis. The left- and right-hand panels show the cross section of the phantom and the result of reconstruction, respectively. In this cross section, irregularities have elongated shape. The quality of reconstruction is also high.

Fig. 11 shows the plot of the cross section of $v\,(x, y, z)$ along the AA line in Fig. 8(b) as a function of the x coordinate. The dashed line corresponds to the exact solution. As is evident from the figure, our developed algorithms can reconstruct not only the shape of the irregularity, but also recover the absolute velocity values with sufficient accuracy.

We adopted $c^{(0)} = const$ as the initial approximation in all computations. Fig. 12 demonstrates the dynamics of the variation of the image of velocity function as a function of the number of iterations $n = 5, 15, 105$.

Table 1 lists the values of the residual functional and the computing time for 1, 5, 15, 105, and 230 iterations. As is evident from the table, the residual functional decreases by a factor of 50 in 105 iterations.

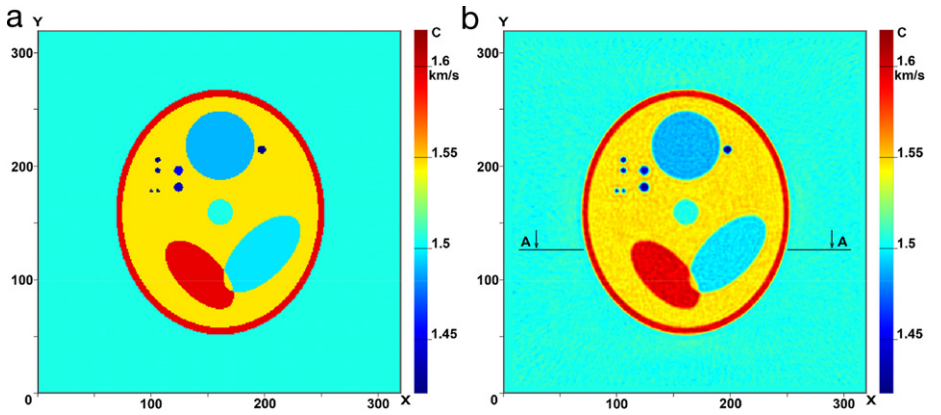

Fig. 8. (a, b). The left- and right-hand panels show the cross sections of the phantom of the 3D object and the reconstructed cross sections of the 3D object, respectively. The cross sections are perpendicular to the Z axis.

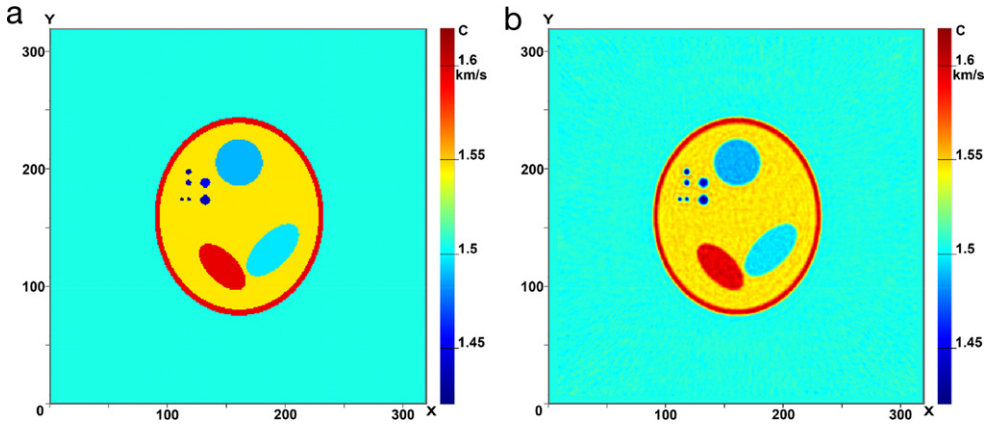

Fig. 9. (a, b). The left- and right-hand panels show the cross sections of the phantom of the 3D object and the reconstructed cross sections of the 3D object, respectively. The cross sections are perpendicular to the Z axis.

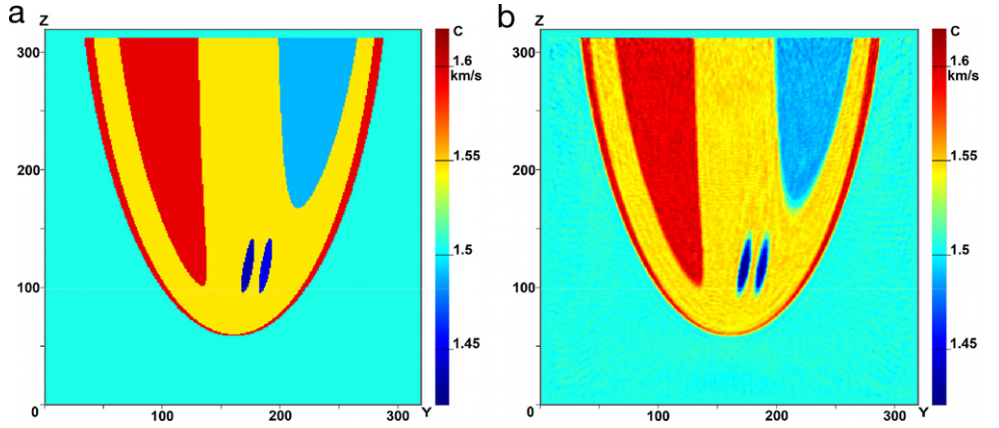

Fig. 10. (a, b). The left- and right-hand panels show the cross sections of the phantom of the 3D object and the reconstructed cross sections of the 3D object, respectively. The cross sections are perpendicular to the Z axis.

The 10^{-4} value of the residual functional corresponds to a $\sim$0.1% error of detector signals. Fig. 13 shows the plot of the residual functional as a function of the number of iterations. The steepest descent method ensures monotonic decrease of the residual functional. The residual functional first decreases rather rapidly, and then the rate of decrease declines appreciably with the increasing number of iterations.

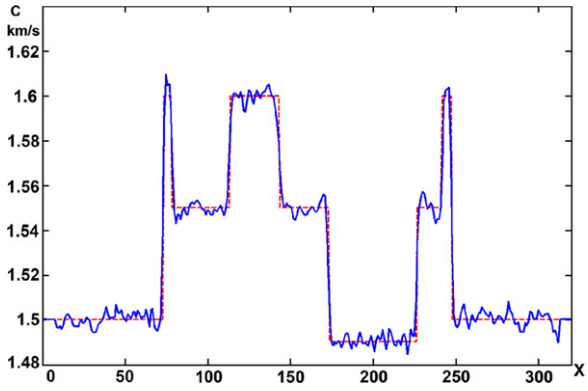

Fig. 11. Plot of the cross section along the AA line in Fig. 8(b).

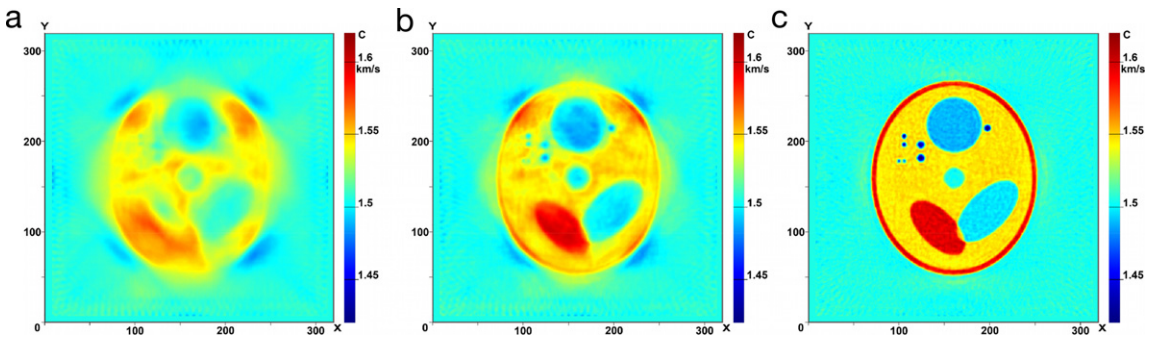

Fig. 12. (a–c). Results of simulations: 5 iterations (a), 15 iterations (b), and 105 iterations (c).

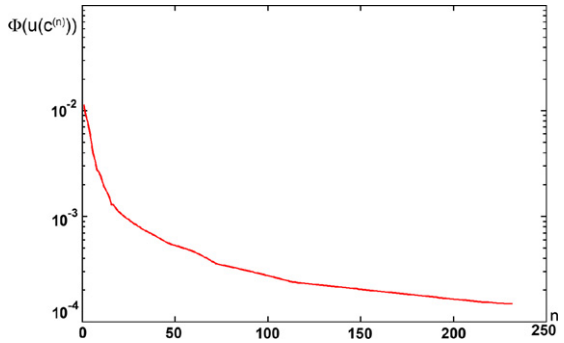

Fig. 13. Residual functional as a function of the number of iterations.

A natural question arises: how the number of sources relates to that of receivers? In this paper, we analyze 3D tomographic schemes with few sources and many receivers. From the mathematical viewpoint the interreceiver distance can be made arbitrarily small in the case of a fixed number of sources. The smaller is the detector size, the better and the physical size of the detector is the only limitation. Detectors with sizes on the order of $\lambda/2$ for $\lambda = 5$ mm are actually producible. Increasing the interreceiver distance is a problem. The results of reconstruction degrade substantially in the case of six sources and about 5λ interreceiver distance, and this degradation does not depend on the algorithms employed, but is rather an inherent property of the problem. How to address this situation if the interreceiver distances are fixed and equal to, e.g., 5λ? There is only one solution: to increase the number of sources. Algorithms developed for solving inverse problems of ultrasound tomography in 3D formulation can be used to determine, via mathematical modeling, the number (and positions) of sources needed to ensure the given quality of reconstruction.

Incomplete angle range.

Standard schemes of ultrasound tomography, when used both in the two- and three-dimensional version, assume that the object can be sounded from any side. It is the fundamental principle for X-ray tomography. We obtained similar results for 2D ultrasound tomography problems with complete angle range in our earlier paper [18].

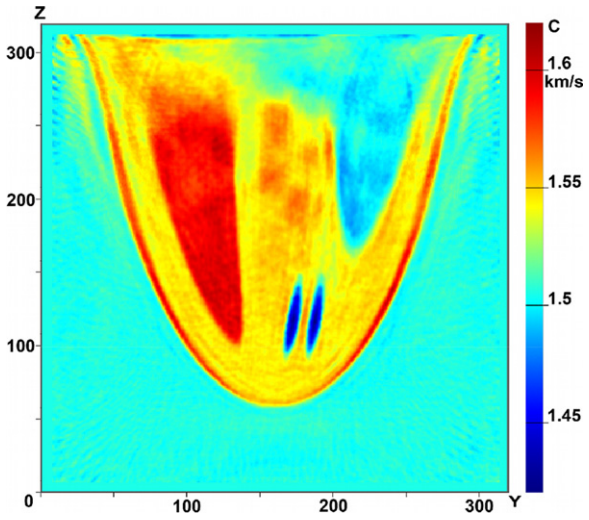

Fig. 14. Reconstructed cross section along the Z axis in the incomplete angle range scheme. Five radiation sources are used.

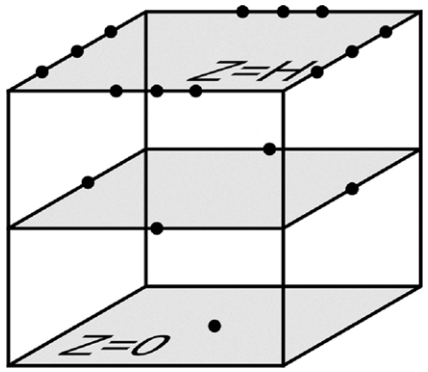

Fig. 15. Arrangement of sources in the experiment with incomplete range of angle data.

A distinguishing feature of ultrasonic tomography problem when applied to diagnosing breast cancer is the incomplete range of data angles. We assume that neither sources nor receivers can be located in the $z \geq H$ region.

Simulations presented in Fig. 14 show that the use of a source layout similar to that shown in Fig. 6 (i.e., with sources located at the centers of all faces of the cube except for $z = H$) is not efficient. Fig. 14 shows the reconstructed cross section similar to that presented in Fig. 11, which passes through the irregularity studied in the plane perpendicular to the X axis. As is evident from the figure, the quality of reconstruction in the $z \geq H/2$ domain is rather low inside the cone with the base located on the $z = H$ face.

The quality of reconstruction can be improved substantially by putting more sources near the $z = H$ plane, like, e.g., shown in Fig. 15.

Fig. 16(a–c) shows the reconstructed cross sections of $v(x, y, z)$ in the scheme with incomplete range of angle data in the planes perpendicular to the Z axis and coinciding with those shown in Figs. 7–9. Fig. 17 shows the reconstructed cross section of $v(x, y, z)$ in the scheme with incomplete range of angle data in the plane perpendicular to the Z axis and coinciding with those shown in Fig. 10. Fig. 15 shows the arrangement of sources. In the case of the specially chosen arrangement of sources, like in Fig. 15, the reconstructed cross sections are practically indistinguishable from the results obtained with complete data range. A more detailed comparison of the images shows that they coincide well for all z_i up to $z_i = H - 1$ mm inclusive, i.e., real differences exist only on $z = H$. This is a rather optimistic result.

It is clear that given the reconstructed function $v(x, y, z)$ as a three-dimensional function specified on a mesh, we can reconstruct the cross section of this function in any plane, which must not necessarily be parallel to any coordinate plane. Fig. 18 shows the cross section of function $v(x, y, z)$ by an inclined plane. There are certain problems related to interpolation and they are due to the misalignment of meshes. It is a purely technical problem that can addressed, e.g., by using splines.

Let us mention some data characterizing the potential of supercomputers in solving problems of ultrasonic tomography. For our simulations we used a GPU-based supercomputer (17 NVIDIA Tesla X2070 GPUs). It took about three hours to solve the inverse problem of the reconstruction of speed function $v(x, y, z)$ as a function of three variables in the case of 17 sources (incomplete range of angle data).

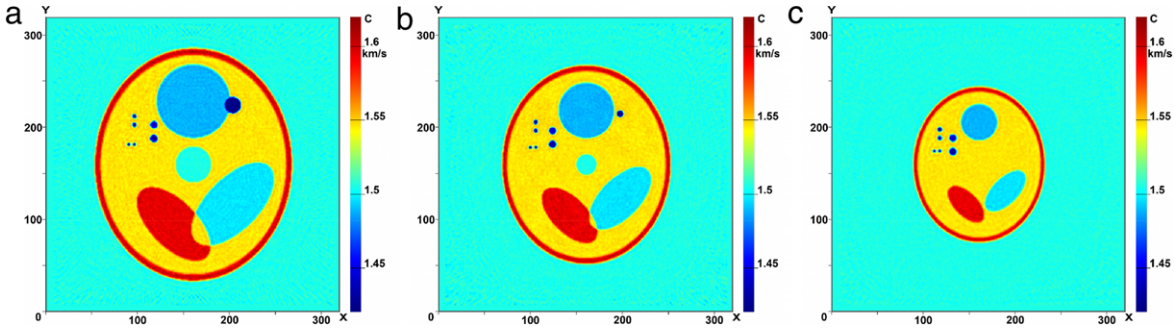

Fig. 16. (a–c). Reconstructed cross sections of the 3D object along the Z axis in the model with incomplete angle range. In this case, 17 radiation sources are used of which 12 are located near the $z = H$ plane.

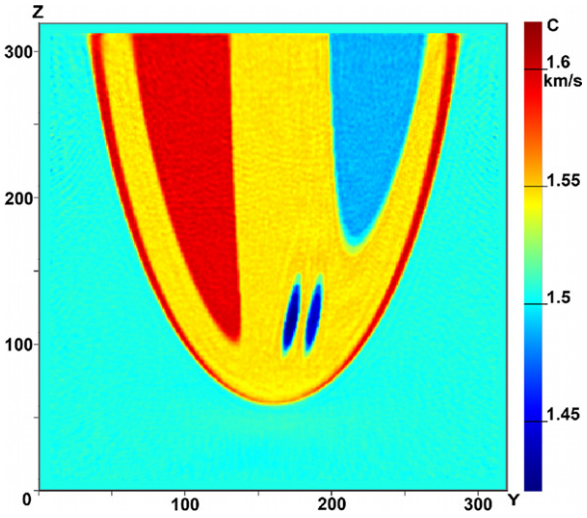

Fig. 17. Reconstructed cross section of the 3D object in the model with incomplete angle range. The cross section is parallel to the Z axis. In this case, 17 radiation sources are used of which 12 are located near the $z = H$ plane.

6. Conclusion and discussion

(1) This work focuses on the development of efficient methods for solving inverse problems of 3D ultrasound tomography as coefficient inverse problems for the wave equation. The inverse problem consists in determining the unknown wave propagation speed as a function of coordinates in the 3D space. Unlike the standard tomographic approach, where the 3D object is analyzed by its two-dimensional cross sections, in this paper we develop algorithms for reconstruction of the three-dimensional, function $v(x, y, z)$. The 3D model is more realistic from the physical viewpoint. The layer-by-layer model performs excellently in X-ray tomography. Model computations show that layer-by-layer model can also be used in ultrasound tomography. However, it produces geometric distortions and artifacts, which are primarily due to refraction effects. Furthermore, the layer-by-layer model cannot account for the rereflection of inhomogeneity fragments in different layers.

(2) Computationally, solving inverse problems of wave tomography in terms of a 3D model is a much more challenging task compared to the layer-by-layer approach. The main achievement of this study is that we demonstrate that all the difficulties arising in numerical implementations of 3D algorithms are addressable. A specific feature of wave tomography is incomplete data range. This situation arises when the object is not sounded from all directions. The worst case scenario is when the object is sounded only from one side of the plane, like, e.g., in standard ultrasound examinations in medicine, seismology, etc. The situation is much better in problems of ultrasound tomography when applied for diagnosing breast cancer, because the object cannot be sounded only from side. We propose efficient algorithms to address the tasks of 3D ultrasound tomography with incomplete data range.

(3) The algorithms developed open up ample opportunities for designing 3D tomographs. Optimization of parameters and measurement schemes is an important point in the design of ultrasound tomographs. We demonstrate with model problems that a proper choice of the locations of few sources allows images to be reconstructed with high accuracy even in the case of incomplete data in tomographic schemes without elements of rotation.

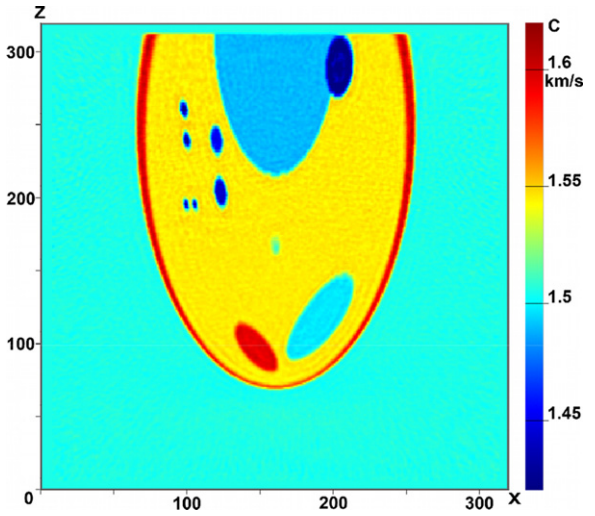

Fig. 18. Reconstructed cross section of the 3D object in an inclined plane in the model with incomplete angle range. The cross section is parallel to the Z axis. In this case, 17 radiation sources are used of which 12 are located near the $z = H$ plane.

(4) The choice of the initial approximation is the major issue to be addressed in approximate solutions of nonlinear problems. Numerous computations of model problems in the parameter domain considered showed that our algorithms solve the direct problem efficiently in iterative schemes starting with the initial approximation $v(x, y, z) = const$. This is a natural choice, because, on one hand, it requires no additional computations, and, on the other hand, the sound propagation speed both in healthy tissue and in neoplasia is within $\pm$10–15% of the sound speed in water.

(5) Currently, Internet makes supercomputers accessible for the researchers. The algorithms developed in this study match well with the structure of GPU supercomputers.

Acknowledgments

It is our pleasant duty to thank Prof. Vl.V. Voevodin for numerous discussions of the work. We are also grateful to Academician V.A. Kubyshkin, Director of Vishnevsky Institute of Surgery of the Russian Academy of Medical Sciences, for the advice concerning medical aspects of the diagnosis of oncological deceases.

This work was supported by the Russian Foundation for Basic Research (project no. 12-07-00304-a).

References

[1] N. Duric, P. Littrup, L. Poulo, A. Babkin, R. Pevzner, E. Holsapple, O. Rama, C. Glide, Detection of breast cancer with ultrasound tomography: first results with the Computed Ultrasound Risk Evaluation (CURE) prototype, Med. Phys. 34 (2007) 773–785.
[2] D.H. Chambers, J. Mast, S.G. Azevedo, F. Wuebbeling, F. Natterer, N. Duric, P. Littrup, E. Holsapple, Diagnostic analysis of ultrasound data, U.S. Pat., 6,984,210, 2006.
[3] H. Gemmeke, A. Menshikov, D. Tchernikovski, L. Berger, G. Göbel, M. Birk, M. Zapf, N.V. Ruiter, Hardware setup for the next generation of 3d ultrasound computer tomography, IEEE NSS MIC (2010).
[4] S.A. Johnson, M. Berggren, D.T. Borup, B.K. Hanover, R. Hanover, M. Kammeyer, S.C. Olsen, J. Pattee, F.L. Setinsek, K.D. Stewart, J.W. Wiskin, Breast scanning system, U.S. Patent, 7,771,360, 2005.
[5] N.V. Ruiter, G.F. Schwarzenberg, M. Zapf, A. Menshikov, H. Gemmeke, Results of an experimental study for 3D ultrasound CT, in: NAG/DAGA 2009 International Conference on Acoustics 1 305–309.
[6] D.P. Dione, L.H. Staib, W. Smith, Three-dimensional ultrasound computed tomography imaging system, U.S. Pat. 7,025,725, 2006.
[7] R. Stotzka, W.A. Kaiser, H. Gemmeke, Ultrasonic tomograph, U.S. Pat. 6,786,868, 2004.
[8] T.A. Bryan, B.E. Holtz, G.F. Perleberg, F.P. Diani, G.S. Hardie, J.C. Robertson, High-resolution three dimensional ultrasound imaging device, U.S. Pat. 5,673,697, 1997.
[9] C.K. Glide, N. Duric, P. Littrup, Novel approach to evaluating breast density utilizing ultrasound tomography, Med. Phys. 34 (2007) 744–753.
[10] C.K. Glide-Hurst, N. Duric, P. Littrup, Volumetric breast density evaluation from ultrasound tomography images, Med. Phys. 35 (2008) 3988–3997.
[11] L. Huang, Y. Quan, Sound-speed tomography using first-arrival transmission ultrasound for a ring array, Proc. SPIE Med. Imaging (2007) 6513.
[12] S. Schmidt, N. Duric, C. Li, O. Roy, Z.F. Huang, Modification of Kirchhoff migration with variable sound speed and attenuation for acoustic imaging of media and application to tomographic imaging of the breast, Med. Phys. 38 (2011) 998–1007.
[13] Ö. Yilmaz, Seismic Data Analysis: Processing, Inversion, and Interpretation of Seismic Data, in: Investigations in Geophysics, vol. 10, Society of Exploration Geophysicists, Tulsa, OK, 2001.
[14] O. Roy, I. Jovanovi'c, A. Hormati, R. Parhizkar, M. Vetterli, Sound speed estimation using wave-based ultrasound tomography: theory and gpu implementation, in: Proc. SPIE 7629, Medical Imaging 2010: Ultrasonic Imaging, Tomography, and Therapy, 76290J.
[15] R.J. Lavarello, M.L. Oelze, Tomographic reconstruction of three-dimensional volumes using the distorted born iterative method, IEEE Trans. Med. Imaging 28 (2009) 1643–1653.
[16] A. Backushinsky, A. Goncharsky, S. Romanov, S. Seatzu, On the identification of velocity in seismics and in acoustic sounding, pubblicazioni dell'istituto di analisa globale e applicazioni, in: Problemi Non Ben Posti ed Inversi, N 71, Firenze, 1994.
[17] A.V. Goncharskii, S.L. Ovchinnikov, S.Yu. Romanov, On the one problem of wave diagnostic, Moscow Univ. Comput. Math. Cybernet. 34 (1) (2010) 1–7.
[18] A.V. Goncharsky, S.Y. Romanov, Supercomputer technologies in inverse problems of ultrasound tomography, Inverse Probl. 29 (2013) 075004.

[19] L. Beilina, M.V. Klibanov, Approximate Global Convergence and Adaptivity for Coefficient Inverse Problems, Springer, New York, 2012.
[20] J. Wiskin, D.T. Borup, S.A. Johnson, M. Berggren, Non-linear inverse scattering: high resolution quantitative breast tissue tomography, J. Acoust. Soc. Am. 131 (2012) 3802–3813.
[21] M. André, J. Wiskin, D. Borup, S. Johnson, H. Ojeda-Fournier, L. Olson, Quantitative volumetric breast imaging with 3D inverse scatter computed tomography, Conf. Proc. IEEE Eng. Med. Biol. Soc. (2012) 1110–1113.
[22] F. Natterer, An algorithm for 3D ultrasound tomography, in: Inverse Problems of Wave Propagation and Diffraction, in: Lecture Notes in Physics, vol. 486, 1997, pp. 216–225.
[23] A.V. Goncharskii, S.Yu. Romanov, On a three-dimensional diagnostics problem in the wave approximation, Comput. Math. Math. Phys. 40 (2000) 1308–1311.
[24] G. Chavent, Deux resultats sur le probleme inverse dans les equations aux derivees partielles du deuxieme ordre an t et sur l'unicite de la solution du probleme inverse de la diffusion, C. R. Acad. Sci. 270 (1970) 25–28.
[25] F. Natterer, F. Wubbeling, A propagation–backpropagation method for ultrasound tomography, Inverse Probl. 11 (1995) 1225–1232.
[26] A.V. Goncharskii, S.Yu. Romanov, Two approaches to the solution of coefficient inverse problems for wave equations, Computational Mathematics and Mathematical Physics 52 (2012) 245–251.
[27] F. Natterer, Incomplete data problems in wave equation imaging, Inverse Probl. Imaging 4 (2010) 685–691.
[28] F. Natterer, Reflectors in wave equation imaging, Wave Motion 45 (2008) 776–784.
[29] A.B. Bakushinsky, A.V. Goncharsky, Ill-posed Problems. Theory and Applications, Kluwer Academic Publ., Dordrecht, 1994.
[30] L. Beilina, M.V. Klibanov, M.Yu. Kokurin, Adaptivity with relaxation for ill-posed problems and global convergence for a coefficient inverse problem, J. Math. Sci. 167 (2010) 79–325.
[31] A.N. Tikhonov, A.V. Goncharsky, V.V. Stepanov, A.G. Yagola, Numerical Methods for the Solution of Ill-posed Problems, Kluwer Academic Publ., Dordrecht, 1995.
[32] B. Engquist, A. Majda, Absorbing boundary conditions for the numerical simulation of waves, Math. Comp. 31 (1977) 629.
[33] Vl.V. Voevodin, S.A. Zhumatiy, S.I. Sobolev, A.S. Antonov, P.A. Bryzgalov, D.A. Nikitenko, K.S. Stefanov, Vad.V. Voevodin, Practice of "Lomonosov" Supercomputer, Open Systems J. Open Systems Publ., Moscow, 2012, No.7. http://www.osp.ru/os/2012/07/13017641/ (in Russian).
[34] V.V. Varadan, Y. Ma, V.K. Varadan, A. Lakhtakia, Scattering of waves by spheres and cylinders, in: Field Representations and Introduction to Scattering, Amsterdam, 1991.
[35] T.S. Angell, R.E. Kleinman, F. Hettlich, The resistive and conductive problems for the exterior Helmholtz equaion, SIAM J. Appl. Math 50 (1990) 1607–1622.